2

Direct Numerical Simulations of Compressible Vortex Flow Problems

S.A. Karabasov[1] and V.M. Goloviznin[2]
[1]*University of Cambridge Department of Engineering*
[2]*Moscow Institute of Nuclear Safety, Russian Academy of Science*
[1]*UK*
[2]*Russia*

1. Introduction

Vortical flows are one of the most fascinating topics in fluid mechanics. A particular difficulty of modelling such flows at high Reynolds (Re) numbers is the diversity of space and time scales that emerge as the flow develops.

For compressible flows, in particular, there are additional degrees of freedom associated with the shocks and acoustic waves. The latter can have very different characteristic amplitudes and scales in comparison with the vorticity field. In case of high Re-number flows, the disparity of the scales becomes overwhelming and instead of Direct Numerical Simulations (DNS) less drastically expensive Large Eddy Simulations (LES) are used in which large flow scales are explicitly resolved on the grid and the small scales are modelled.

For engineering applications, examples of unsteady vortical flows include the interaction of wakes and shocks with the boundary layer in a transonic turbine and vorticity dissipation shed due to the temporal variations in blade circulation that can have a profound loss influence and affect the overall performance of a turbomachine (e.g., Fritsch and Giles, 1992; Michelassi et al, 2003). Another example is dynamics and acoustics of high-speed jet flows that is affected by the jet inflow conditions such as the state of the boundary layer at the nozzle exit (e.g., Bogey and Bailly, 2010). The computational aspects involved in the modelling of such complex flows, typically, include the issues of high-resolution numerical schemes, boundary conditions, non-uniform grids and the choice of subgrid scale parameterization in case of LES modelling.

Stepping back from this complexity to more idealised problems, two-dimensional (2D) vortex problems are a key object for testing different modelling strategies. Such reduced-order systems play an important role in the understanding of full-scale flow problems as well as in benchmarking of computational methods.

One example of such important idealised systems is isolated vortices, their interaction with acoustic waves and also nonlinear dynamics when interacting with each other. In particular, such vortical systems are a classical problem in the theory of sound generation and scattering by hydrodynamic non-uniformities (e.g., Kreichnan, 1953; Howe, 1975)

The structure of the chapter is the following. In part I, an outline of unsteady computational schemes for vortical flow problems is presented. In part II, the test problem of a stationary inviscid vortex in a periodic box domain is considered and a few numerical solutions

obtained with unsteady Eulerian schemes are discussed. Part III is devoted to the sound scattering by a slowly decaying velocity field of a 2D vortex. In part IV, the canonical problem of 2D leapfrogging vortex pairs is considered and numerical solutions based on the Eulerian and Lagrangian approach are discussed.

2. Numerical methods for solving unsteady flow problems sensitive to vortex dynamics

Numerical dissipation and dispersion are typical drawbacks of the Eulerian computational schemes (e.g., Hirsch, 2007). These drawbacks are partially overcome in the Lagrangian and mixed Eulerian-Lagrangian methods, which describe flow advection by following fluid particles, rather than by considering fixed coordinates on the Eulerian grid (e.g., Dritschel et al, 1999). A remarkable property of the Lagrangian methods is that they are exact for linear advection problems with a uniform velocity field, therefore, in principle, their accuracy is limited only by the accuracy of solving the corresponding Ordinary Differential Equations (ODEs), rather than by the accuracy of solving the full Partial Differential Equations (PDEs), which is the case for the Eulerian schemes. This class of methods can be very efficient for simulations, which involve multiple contact discontinuities, e.g., in the context of multi-phase flows and strong shock waves (e.g., Margolin and Shashkov, 2004). However, for the problems where vorticity plays an important role, the standard Lagrangian-type methods have to be adjusted, after not many Lagrangian steps, by some ad-hoc 'repair' or 'contour surgery' procedure. The 'repair' procedure can be actually viewed as a special kind of numerical dissipation that is needed to stabilise the numerical solution.

For the Eulerian schemes, one of the frequently used approaches for improving the numerical dissipation and dispersion properties is based on using central schemes of high-order spatial approximation. The optimized schemes employ a non-conservative form of the governing equations, and, typically, use large computational stencils to replicate the spectral properties of the linear wave propagation in the (physical) space-time domain (Lele, 1992; Tam and Webb, 1993; Bogey and Bailly, 2004). By construction, such methods are particularly efficient in handling linear wave phenomena. The optimized finite-difference methods were developed to overcome typical problems of spectral and pseudo-spectral methods by handling non-periodic boundary conditions and large flow gradients which they handle with the use of hyper diffusion.

On the other hand, there is another popular approach, based on the conservation properties of the governing equations, that forms the basis for the so-called shock-capturing schemes. This is the family of methods based on the quasi-linear hyperbolic conservation laws (Roe, 1986; Toro, 2001; LeVeque, 2002). For improving the numerical properties in this approach, either a second-order or higher 'variable-extrapolation', or 'flux-extrapolation' techniques are used, such as in Method for Upwind Scalar Conservation Laws (MUSCL, Kolgan, 1972; B.van Leer, 1979), for enhancing linear wave properties of the solution away from the large-solution gradients discontinuities. The time stepping is usually treated separately from the spatial approximation and one popular method for time integration is multi-stage Runge-Kutta schemes (e.g, Hirsch, 2007).

To eliminate spurious oscillations of the solution obtained with the second- or higher-order schemes, in the vicinity of the discontinuities, local non-linear limiter functions are suggested, as, for example, in Totally Variation Diminishing (TVD) schemes (Boris et al.,

1975). By enforcing the TVD property on the solution, the limiter functions introduce implicit numerical dissipation. If the numerical dissipation gets too strong, artificial anti-diffusion terms are added to make the method less dissipative (Harten et al., 1987). The non-oscillatory methods are very attractive for computing flows with shocks. For weakly non-linear flow problems, however, the shock-capturing TVD schemes tend to introduce too much dissipation and for vortical flows, especially in acoustics sensitive applications, the limiters are recommended to switch off (e.g., Colonius and Lele, 2004), i.e., selectively use the non-oscillatory methods only for strong discontinuities.

One notable exception is the so-called Compact Accurately Adjusting high-Resolution Technique (CABARET) (Karabasov and Goloviznin, 2009). CABARET is the extension of Upwind Leapfrog (UL) methods (Iserlis, 1986; Roe, 1998; Kim, 2004; Tran and Scheurer, 2002) to non-oscillatory conservative schemes on staggered grids with preserving low dissipative and low dispersive properties. CABARET is an explicit conservative finite-difference scheme with second-order approximation in space and time and it is found very efficient in a number of Computational Fluid Dynamics (CFD) problems, (Karabasov and Goloviznin, 2007; Karabasov et al, 2009). In comparison to many CFD methods, CABARET has a very compact stencil which for linear advection takes only one computational cell in space and time. The compactness of the computational stencil results in the ease of handling boundary conditions and the reduction of CPU cost. For non-linear flows, CABARET uses a low-dissipative conservative correction method directly based on the maximum principle.

For collocated-grid schemes, the mainstream method of reducing numerical dissipation is to upgrade them to a higher order (typically, by extending its computational stencil). There is a broad range of recommendations on the subject, starting from Essentially or Weighted Essentially Non-Oscillatory schemes (ENO and WENO) (Liu et al, 1994) to Discontinuous Galerkin methods (Cockburn and Shu, 2001). All these methods show significant improvements in terms of preserving the linear flow properties, if compared with the conventional second-order schemes.

For illustration of numerical properties of different Eulerian schemes, Fig 1 shows the comparison of phase speed error and the non-dimensional group speed as a function of grid resolution for several semi-discrete central finite differences. E2, E4, E6 denote standard central differences of the second, fourth and sixth-order, respectively, DRP denotes the fourth order Dispersion Relation Preserving scheme by Tam and Webb; and LUI stands for the sixth order pentadiagonal compact scheme of Pade-type. CABARETx stands for the CABARET dispersion characteristic at various Courant number CFL=x. All solutions are shown as a function of the grid refinement parameter, $N_\lambda=\pi/(k\cdot h)$ and the non-dimensional wavenumber, $k\cdot h$, respectively. Note that the solutions for the second-order discretization are typical of the 'low-order' shock-capturing methods, e.g., the Roe MUSCL scheme, with the limiter switched off. Higher-order central schemes of the 4^{th} and the 6^{th} order are analogues to the high-order shock-capturing methods, such as WENO, in the smooth solution region. The results for two pseudo-spectral optimised dispersion schemes are also shown.

Note that the dispersion errors of semi-discrete schemes correspond to exact integration in time, which neglects the possible increase of dispersion error due to inaccuracies in time marching. For most Courant numbers and for a wide range of grid resolution (7-20 points per wavelength) the dispersion error of the CABARET scheme remains below that of the conventional and optimised fourth-order central finite differences and close to that of the six-order central schemes. Away from the optimal Courant number range (e.g., for

CFL=0.1), the CABARET dispersion error is similar to that of the conventional fourth-order scheme. Fig1b shows that the numerical group speed of central finite-difference schemes on coarse grids is negative that leads to spurious wave reflection and sets the limit to the minimum grid resolution if numerical backscatter is to be avoided (Colonius and Lele, 2004). In comparison with the central schemes, the CABARET group speed remains in the physically correct direction for all wavenumbers, i.e., the non-physical backscatter is always absent.

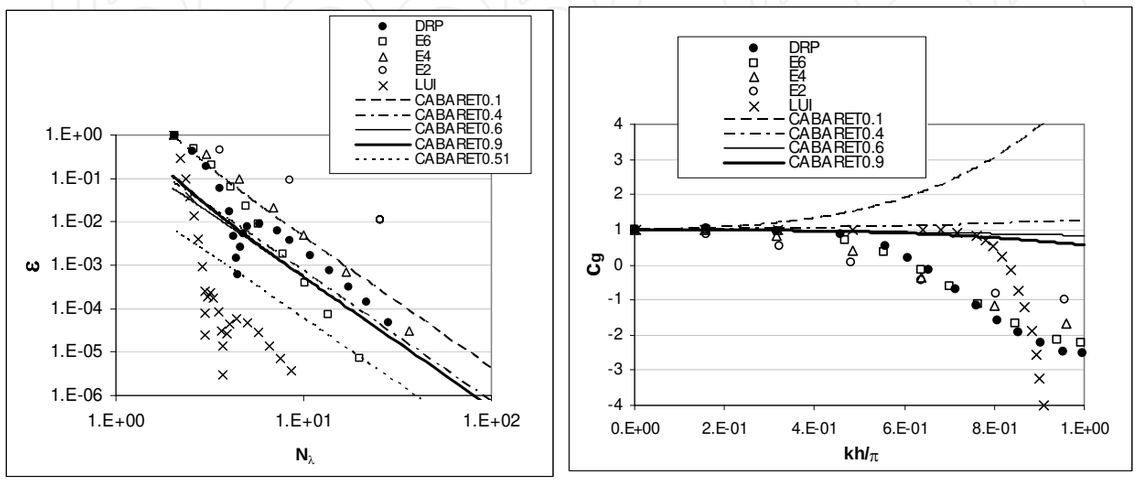

(a) (b)

Fig. 1. Linear wave properties of several spatial finite-difference schemes: (a) phase errors and (b) normalised group speeds.

3. Steady vortex solution in a finite domain

Let's first consider a steady problem of isolated compressible Gaussian vortex in a square periodic domain. The vortex is specified in the centre of the box domain, as a perturbation to a uniform background flow with zero mean velocity $(\rho_\infty, \mathbf{u}_\infty, p_\infty)=(1,0,1)$:

$$\rho' = \rho_\infty \left[\left(1 - \frac{(\gamma-1)}{4\alpha\gamma} \varepsilon^2 \exp\{2\alpha(1-\tau^2)\} \right)^{\frac{1}{\gamma-1}} - 1 \right], u' = \varepsilon\tau \exp\{\alpha(1-\tau^2)\} \sin\theta,$$

$$v' = -\varepsilon\tau \exp\{\alpha(1-\tau^2)\} \cos\theta, p' = p_\infty \left[\left(1 - \frac{(\gamma-1)}{4\alpha\gamma} \varepsilon^2 \exp\{2\alpha(1-\tau^2)\} \right)^{\frac{\gamma}{\gamma-1}} - 1 \right], \quad (1)$$

$$\tau = r/L; r = \sqrt{(x-x_0)^2 + (y-y_0)^2}; \theta = \tan^{-1}((y-y_0)/(x-x_0)), \varepsilon = 0.3, L = 0.05, \alpha = 0.204.$$

To simplify the treatment of external boundary conditions, the box size is set 20 times as large as the vortex radius, L so that the vortex induced velocity vanishes at the boundaries. The vortex field corresponds to a steady rotation that is a stable solution of the governing compressible Euler equations (e.g., Colonius at al, 1994). The characteristic space scale of the problem is the vortex core radius L. It is also useful to introduce the time scale based on the vortex circulation time $T = 2\pi L / \varepsilon \simeq 1.047$.

The analytical solution of the problem is trivial: at all time moments the solution remains equal to the initial conditions. From the viewpoint of unsteady computational schemes, however, preserving the vortex solution on a fixed Eulerian grid that is not specifically tailored to the initial vortex shape tends to be a challenge.

To illustrate the point we consider numerical solutions of this problem obtained with two high-resolution Eulerian methods mentioned in the introduction. These are the Roe-MUSCL scheme with and without TVD limiter (MinMod) and the CABARET method. The former method is based on the third-order MUSCL variable extrapolation in characteristic variables and the third order Runge-Kutta scheme for in time. The latter is based on a staggered space-time stencil and is formally second order. Note that the MinMod limiter used with the Roe MUSCL scheme is more robust for vortical flow computations in comparison with more 'compressive' limiters, e.g., SuperBee, that are better tailored for 1-D shock-tube problems. This is because the former is less subjected to the 'stair-casing' artefacts in smooth solution regions (e.g., see Hirsch, 2007). The Euler equations with the initial conditions (1) are solved on several uniform Cartesian grids: (30x30), (60x60), (120x120) and (240x240) cells. These correspond to the grid density of 1.5, 3, 6 and 12 grid spacings per the vortex core radius, respectively. Figs 2 show the grid convergence of the vorticity solution obtained with the CABARET method at control time t=100. The shape and the peak of the vortex is well preserved on all grids including the coarsest one. For qualitative examination, the kinetic energy integral has been computed $K(t) = \sum_{x,y} \rho u_i u_i$, as a fraction of its initial value $K(0)$. The relative error $\varepsilon(t) = 1 - K(t) / K(0)$ of this nonlinear problem at t =100 shows approximately a linear decay with the grid size: it is 0.011 for grid (30x30), 0.0061 for grid (60x60), and 0.003 for grid (120x120). For the Roe-MUSCL scheme, the solution of the vortex problem is much more challenging. The activation of the TVD limiter leads to a notable solution smearing, which builds up with time, and which affects even the solution on the fine grid (120x120) (fig.3a). It is, therefore, tempting to deactivate the TVD limiter since in the case considered there are no shocks involved. Without the limiter, the Roe-MUSCL scheme initially preserves the vortex shape well (as in fig.3b). However, after a few vortex circulation times, spurious oscillations that correspond to the nonphysical propagation direction of the short scales (cf. fig.1b) grow until they completely contaminate the vortex solution (fig3c).

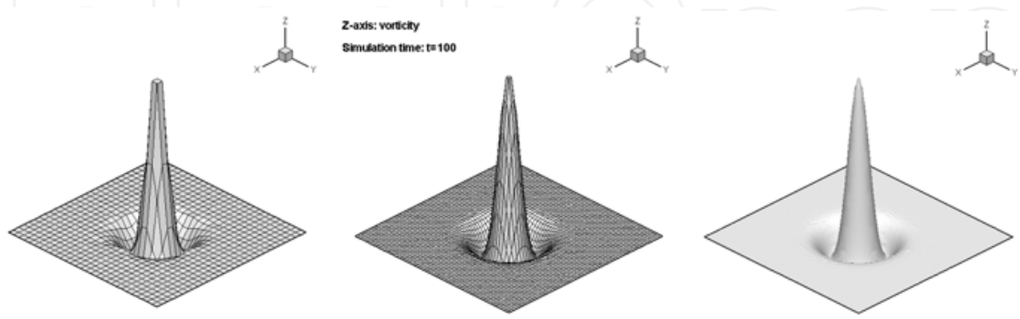

(a) (b) (c)

Fig. 2. Steady compressible Gaussian vortex in a periodic box domain: vorticity levels of the CABARET solution at time t=100 on (a) grid (30x30), (b) grid (60x60) , and (c) grid (120x120).

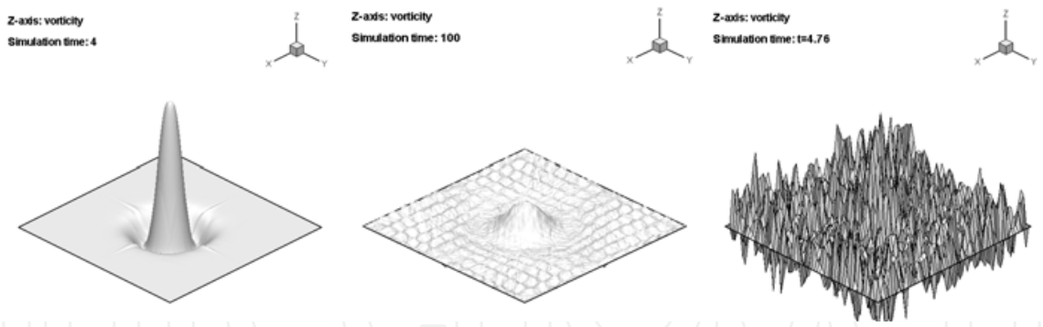

(a) (b) (c)

Fig. 3. Steady compressible Gaussian vortex in a periodic box domain: vorticity levels of the Roe-MUSCL solution on grid (240x240) cells with (a) MinMod limiter at time t=100, (b) MinMod limiter at time t=4, and (c) with the limiter deactivated at time t=5.

4. Sound scattering by a steady vortex

We next consider an isolated viscous-core vortex from Colonius at al (1994) that corresponds to a slowly decaying velocity field of constant circulation $\Gamma_\infty > 0$

$$\begin{aligned} &v_r = 0 \\ &v_\theta = \frac{\Gamma_\infty}{2\pi r}(1-\exp(-\alpha(r/L)^2)) \\ &\alpha = 1.256431,\ \mathrm{M}_{\max} = (v_\theta)_{\max} / c_\infty \end{aligned} \tag{2}$$

where c_∞ is acoustic far-field sound and L is the vortex core radius. The density and pressure field satisfy the usual isentropic relation and the steady tangential momentum equation:

$$\begin{aligned} &p \cdot \rho^{-\gamma} = const; \\ &\frac{\delta p}{\delta r} = \rho \frac{{v_\theta}^2}{r} \end{aligned} \tag{3}$$

The vortex is specified in the centre of an open square Cartesian domain, three sides of which are open boundaries and the forth one corresponds to an incident acoustic wave that is monochromatic with frequency f. and normal to the boundary. The incident wave boundary condition is imposed at distance R=10L from the vortex centre which is offset from the centre of the square computational box domain of linear size 40L.
The velocity perturbations of the incident acoustic wave are several orders of magnitude as small as the maximum velocity of the vortex, u'=1.e-5$(v_\theta)_{\max}$. The problem has two length and time scales associated with the vortex circulation and the acoustic wave. The case of long acoustic wavelength λ=2.5L is considered first.
The solution of the acoustic wave scattered by the vortex is sought in the form of the scattered wave component

$$p' = p - p^{(a)} - \delta p, \quad \delta p = (p^{(v)} - p_\infty) \tag{4}$$

where p is the full pressure field obtained as the solution of the sound wave interaction with the vortex, $p^{(a)}$ is the solution that corresponds to the acoustic wave propagating in the free

space without any hydrodynamic perturbation, $p^{(v)}$ is the steady solution vortex without any incoming acoustic wave, and p_∞ is the pressure at the far field. Note, that from the numerical implementation viewpoint it is preferable to compute the scattered solution in form (5) instead of using $\delta p = (p_{t=0} - p_\infty)$ in order to account for a small systematic approximation error of the round vortex on a rectilinear Cartesian grid.

Colonius et al (1994) obtain the benchmark solution to this problem by using the 6-th order Pade-type compact finite-difference scheme in space and 6-th order Runge-Kutta integration in time with the grid density of 7-8 grid points per vortex radius. The reference solution corresponds to the Navier-Stokes equations at Reynolds number 10^5 integrated over four acoustic wave time periods in the open computational domain with well-tailored numerical boundary conditions to minimise numerical reflections from the boundaries.

It is interesting to compare the reference solution with the results obtained with the CABARET scheme and the third-order Roe-MUSCL-Runge-Kutta method from the previous section. To reduce the numerical dissipation error of the latter, the MinMod limiter has been deactivated. For CABARET, the complete formulation including the nonlinear flux correction is used. For the sake of comparison, the vortex with core Mach number $M_{\max} = 0.25$ is considered. Characteristic-type nonreflecting boundary conditions and grid stretching close to the open boundaries are used to minimise artificial reflections.

Fig.4 shows the computational problem configuration and the distribution of the root-means-square (r.m.s.) of the scattered pressure fluctuations for the CABARET solution, where the vortex centre corresponds to the origin of the system of coordinates.

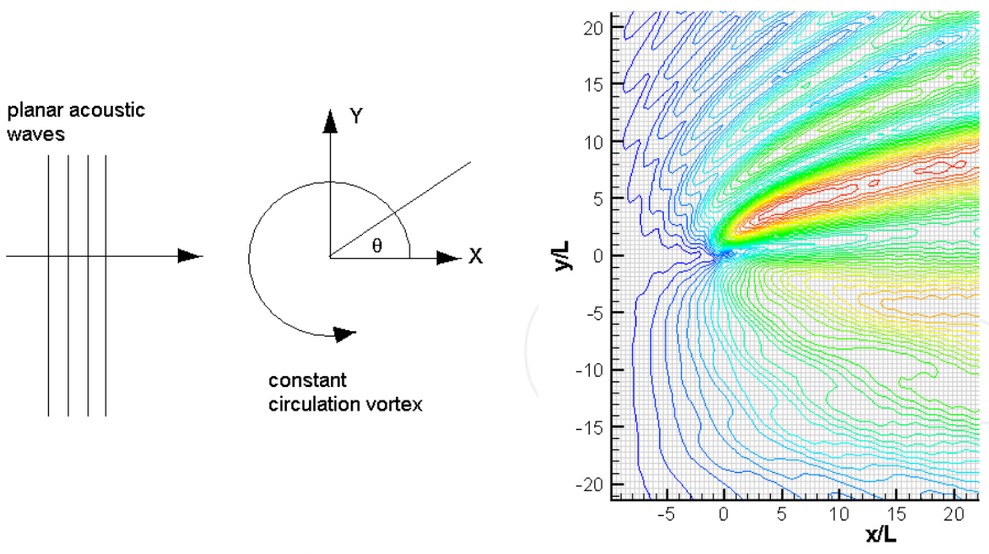

(a) (b)

Fig. 4. Sound wave scattering by a non-zero circulation vortex of M=0.25: (a) problem configuration, (b) computed r.m.s of the scattered pressure field of the CABARET solution on coarse grid of 2.5 cells per vortex core radius.

The main emphasis of this subsection is the effect of non-uniform hydrodynamic flow on sound scattering, hence, the numerical solutions for the scattered pressure field intensity

$r.m.s.(p') = f(R,\theta)$ (acoustic pressure directivity) at a large distance from the vortex centre R=10L are considered. Figs.5 show the acoustic pressure directivity $r.m.s.(p') = f(R,\theta)$ with respect to the polar angle defined anti-clock-wise from the positive x-direction. The comparison of the CABARET solution with the reference solution of Colonius et al (1994) is shown in Fig.5a. To monitor the grid convergence, the Euler equations are solved on a Cartesian grid whose resolution is gradually increasing: (100,100), (200x200) и (400x400) cells (2.5, 5 and 10 grid points per vortex radius, respectively). For CABARET, the r.m.s. distributions on the two finer grids virtually coincide.

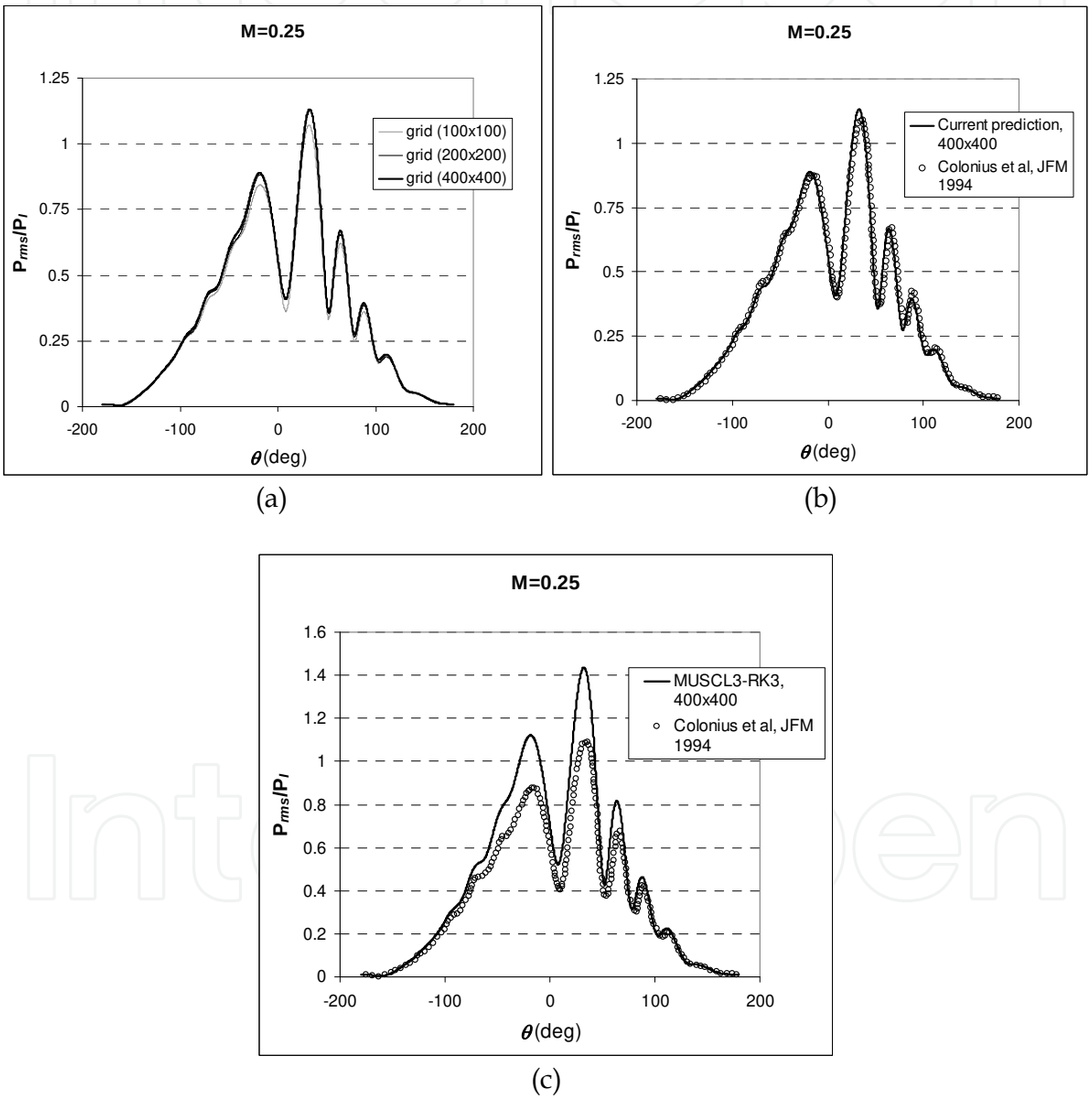

Fig. 5. Sound wave scattering by a vortex: (a) grid convergence of the scattered pressure r.m.s. field of the CABARET solution, (b) comparison of the fine-grid CABARET results with the reference solution of Colonius et al (1994), (c) comparison of the fine-grid 3rd order Roe/MUSCL results with the reference solution of Colonius et al (1994).

For the Roe-MUSCL scheme, the comparison with the reference solution on the finest grid (400x400) is shown in Fig.5c. In comparison to the CABARET results (fig.5a), for the Roe-MUSCL scheme there is some 30% overprediction of the peak sound directivity that is associated with numerical dispersion. Clearly, the acoustic peak corresponds to the downstream vortex direction where the sound waves spend more time inside the strongest vortex-induced hydrodynamic field and which direction is more sensitive to the linear dispersion error of the numerical scheme.

The next case considered is the high frequency acoustic wave imposed as the inflow boundary condition. It is well known (e.g., Kinsler and Frey, 2000) that in the high-frequency limit $\lambda << L$ the Euler equations can be reduced to the ray-theory equations. The latter, for example, describe the effect of focusing and defocusing of acoustic rays as they pass through a non-uniform medium. In particular, the focusing of acoustic rays creates caustics which loci can be found from the solution of eikonal equation (Georges, 1972). On the other hand, caustic locations correspond to the most intense root-mean-square (r.m.s) fluctuations of the pressure field that can be obtained directly from solving the Euler equations.

To illustrate this numerically, let's consider the incident acoustic wave at a high-frequency wavenumber λ =0.076 L and solve the Euler equations with the CABARET method. For this calculation, the computational grid with the resolution of 7-8 cells per acoustic wavelength that corresponds to (1000x1200) grid cell points is used. Fig.6a shows the scattered pressure r.m.s. field obtained from the Euler solution, where the loci of the caustics bifurcating into two branches, as obtained in Colonius at al (1994), are shown. The centre of the vortex corresponds to the origin of the coordinate system. The caustics branches outline the acoustic interference zone that develops behind the vortex. Fig.6b shows the pressure r.m.s. directivity, $r.m.s.(p') = f(R,\theta)$ of the computed solution at distance R=L from the vortex centre. Two grid resolutions are considered, 7 and 14 grid cells per acoustic wavelength. The polar angle variation corresponds to the top half of the computational domain which intersects one of the caustics bifurcation point at ~ 70^0 relative to the incident wave direction.

For the solution grid sensitivity study, the scattered pressure r.m.s. solutions are computed with two grid densities, as shown in Figs 6c,d. It can be seen the main features such as the caustic point location and the peak amplitudes are well captured on both grids. The scattered acoustic pressure solution component is then further used to compute the trajectories of sound rays. The trajectories are defined as the normal to the scattered pressure r.m.s. fronts. In particular, from this vector field, the maximum angle of the acoustic ray deflected by the vortex can be compared with the ray-tracing solution. According to the ray theory, the maximum deflection angle scales linearly with the vortex Mach number.

Fig. 7 shows the maximum deflection angles obtained from the Euler calculation (Euler) and the reference values obtained from the ray-tracing solutions. All solutions are in a good agreement and follow the linear trend expected. In particular, the Euler solution almost coincides with the eikonal solution of Tucker and Karabasov (2009) that corresponds to the same computational domain size. The slight disagreement with the other ray-tracing solutions is likely to be caused by the differences in the domain size, i.e., the proximity of inflow boundary conditions, as discussed by Colonius et al, 1994.

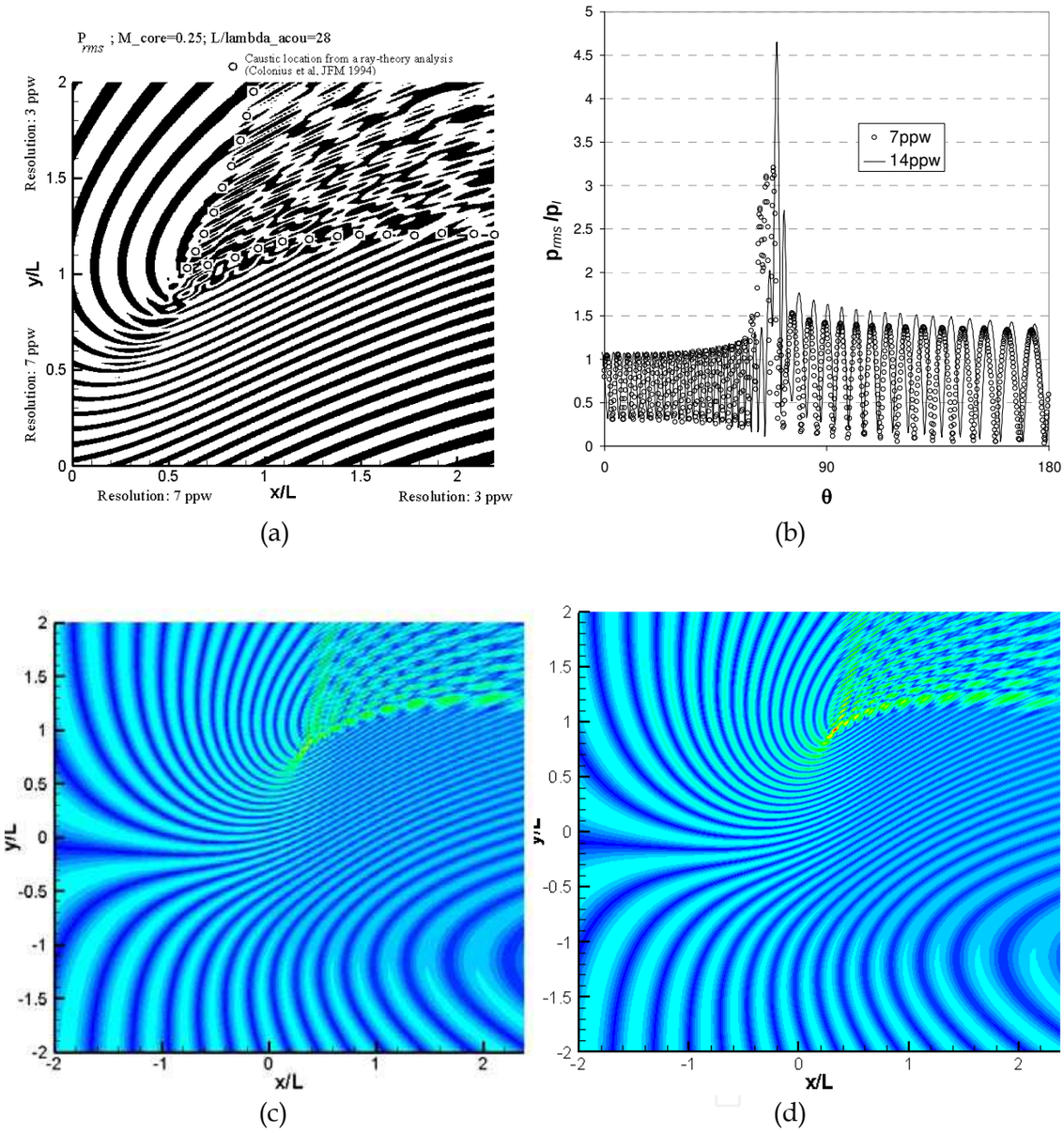

Fig. 6. Euler solution of the sound scattering by a vortex at high frequency: (a) pressure r.m.s. field where the loci of caustic branches are shown with the open symbols, (b) pressure r.m.s. directivity in the top half of the domain for the grid resolutions 7 and 14 cell per acoustic wavelength (7 ppw and 14 ppw); the scattered pressure r.m.s. for vortex core Mach number M_{max}=0.295 with the grid density of (c) 7 cells per acoustic wavelength and (d) 14 cells per acoustic wavelength.

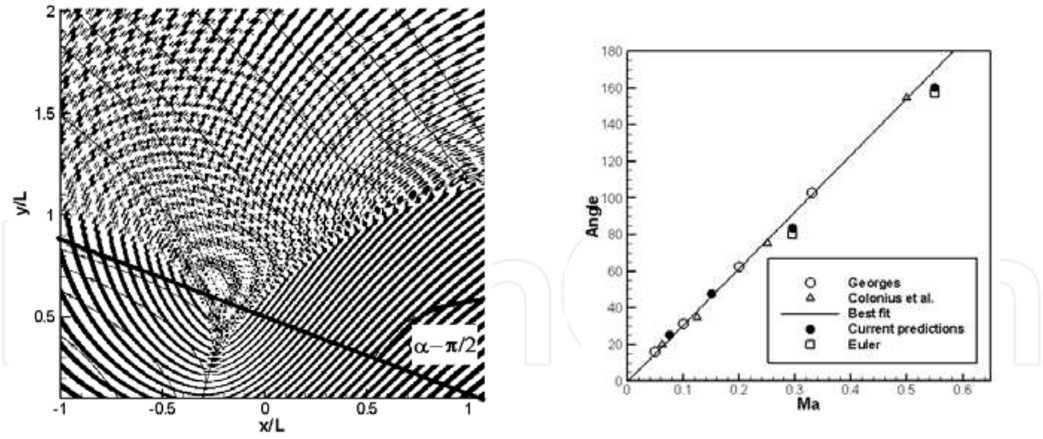

(a) (b)

Fig. 7. Extracting sound ray trajectories from the Euler solution (a) for vortex Mach number 0.55 and (b) comparing the extracted maximum ray deflection angle as a function of various vortex Mach numbers with several ray-tracing solutions.

5. Dynamics of counter-rotating vortices

As the final example, we consider the test problem of interacting counter-rotating vortices that involves both their nonlinear dynamics and, as a by-product, sound generation. For small viscosity, the direct simulation of vortex dynamics and acoustics by solving the compressible Navier-Stokes equations on a Eulerian grid is a challenging problem because of the thin vorticity filaments that are generated as the process evolves in time. These are difficult to capture because of numerical dissipation-dispersion problems mentioned in the introduction. In the literature, examples of flow simulations have Reynolds number, as defined based on the velocity circulation, in the range of 1000-4000 (e.g., Inoue, 2002). Eldridge (2007) manages to accurately compute the problem of dynamics and acoustics of counter-rotating vortex pairs at a high Reynolds number, Re=10000 with the use of a Lagrangian vortex particle method. In the latter, the governing fluid flow equations are solved in a non-conservative form and the advected vortex solution is regularly reinitialised on a Eulerian grid to reduce the complexity of thin vorticity filaments and stabilise the solution. In the present subsection, the problem of counter-rotating vortices is solved on a fixed Eulerian grid for the range of Reynolds numbers, Re=5000-10000 with the conservative Navier-Stokes CABARET method.

Fig. 8 shows the problem setup. Four viscous-core counter-rotating vortices are initiated in an open domain. Each of the vortices has a constant velocity circulation at infinity $\pm\Gamma, \Gamma > 0$ and a Gaussian distribution of the vorticity with the core radius r_0

$$\xi = \frac{1.25\Gamma}{\pi r_0^2} e^{-1.25\left(\frac{r}{r_0}\right)^2} \tag{5}$$

where $\Gamma = 0.24\pi\delta a_\infty$ that corresponds to the vortex core Mach number $M_0 = 0.3$ and $\delta_x = \delta_y = \delta = \frac{10}{3} r_0$ is half-distance between the adjacent vortex centres. In non-dimensional variables, the flow parameters at infinity are taken to be $p_\infty = 1, \rho_\infty = 1$ and $\delta = 0.2$. The initial location of the centre of mass of the system corresponds to **x**=0.

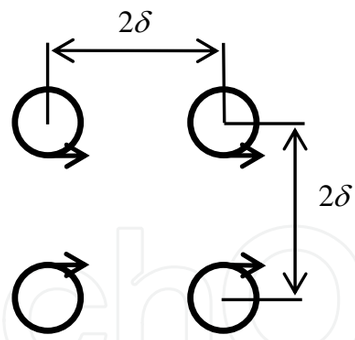

Fig. 8. Problem configuration for two counter-rotating vortex pairs.

The vortex system undergoes a jittering motion with one vortex pair sleeping through the other and taking turns. The centre of mass travels at a positive subsonic speed, which corresponds to the right horizontal direction in Fig.8. After each sleep-through, the distance between the vortices decreases until they finally coalesce and continue the movement as a single core. By using a point-vortex approximation with neglecting viscous effects, the dynamics of the vortex system before coalescence can be described by the classical analytical solution of Hicks (1922). This solution gives the following expressions for the centre mass velocity $\overline{U}$ and the slip through period T_p of the vortex system:

$$. \overline{U} = \frac{\delta_y \cdot \Gamma}{4\pi\delta_x{}^2}\left[\frac{k^2 E(k)}{E(k)-(1-k^2)K(k)}\right], T_p = \frac{32\pi\,\delta_x{}^2}{\Gamma k^2(1+k)}\Big(E(k)-(1-k^2)K(k)\Big) \tag{6}$$

where k=1/[1+(δ_y / δ_x)²]=0.5 and $K(k), E(k)$ are the complete elliptic integrals of the first and second kind. For the specified parameters of the model, the centre mass velocity and slip-through period are

$$T_p = \frac{54.46\delta^2}{\Gamma} = 12.21,\ \overline{U} = \frac{0.1437\cdot\Gamma}{\delta} = 0.1282\,. \tag{7}$$

The velocity of the centre mass corresponds to the Mach number $M_\infty = 0.1083$.

Because of the problem symmetry with regard to axis y=0, one-half of the computational domain is considered with the symmetry boundary condition. The problem is solved in the inertial frame of reference which velocity with regard to the absolute frame equals the velocity of the centre of mass, $\overline{U}$. The latter is available from the analytical point-vortex solution. Because of this choice the centre of mass is approximately stationary in the reference coordinate system. The latter is helpful for minimising the size of the computational domain.

The computational domain of size 440δ x 220δ (axially times vertically) is covered by a Cartesian grid that has a uniform grid spacing in the central block (60δ x 30δ). Exponential grid stretching is applied near the outer boundaries to reduce numerical reflections (Fig.9). Three grid resolutions are considered: 6, 9 and 12 grid cells per vortex core radius.

Initial conditions in conservation variables are computed in the following way. By combining the initial vorticity distribution (5) with the solenoidal velocity field condition, the velocity field is computed from solving the Laplace equation for velocity potential. The

resulting velocity field is substituted to the momentum equations in conservation variables that are then integrated numerically with the use of the isentropic flow relation between pressure and density.

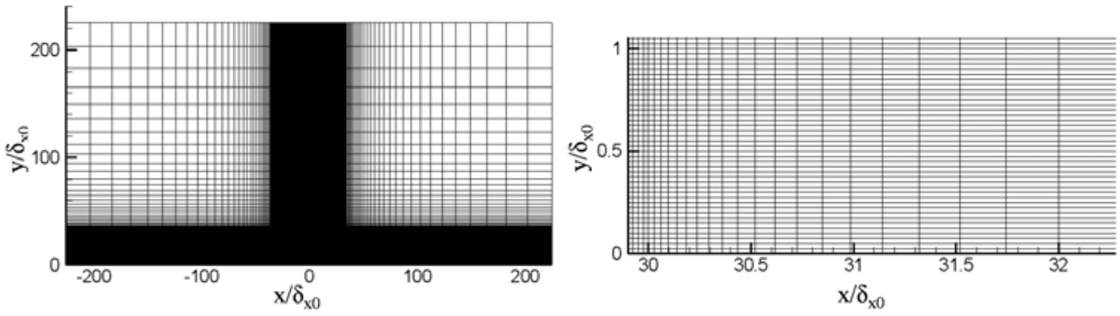

(a) (b)

Fig. 9. Computational grid: (a) full domain view and (b) zoom in the beginning of the grid stretching zone.

Fig.10 shows the time evolution of vorticty field of the system as the vortex pairs sleep through each other. The grid density is 6 grid cells per vortex radius and the Reynolds number of the CABARET simulation is 9400. This particular Reynolds number is chosen as the best match for the reference Lagrangian particle solution of Eldridge (2007) that corresponded Re=10000. The 5% difference in the Reynolds numbers may be attributed to the differences in numerical approximation of viscous terms in the momentum and energy equations in the conservative CABARET and the non-conservative vortex particle method.

For Re=9400, the vortex pairs merge after 4 sleep-through events. The sleep-though events correspond to Fig10(c),(d),(e),(f). For Re=5000, the coalescence happens earlier in comparison with the Re=9400 case: for the lower Re-number the vortices coalesce already after 3 sleep-throughs. This change can be compared with results for the fully inviscid follow case calculation that was conducted with the same CABARET Euler method. In the latter case the vortices manage to undergo 6 sleep-through events before coalescence. The capability of the CABARET model to capture the qualitative differences between the Re=9400 and the fully inviscid solution is noted as a good indication of how low-dissipative the method is.

To zoom into the flow details, Fig.11 compares instantaneous vorticity contours obtained from the CABARET solution at two grid resolutions, 6 and 12 cells per core radius, with the reference Lagrangian particle solution from Eldridge (2007) at one time moment. This time moment corresponds to the last vortex sleep-through before the coalescence. At this time the vortices are very close and strongly interact with each other through fine vorticity filaments. For all three solutions, the same contour levels are plotted that show a good agreement down to a small detail.

It is also interesting to compare the 2D solution computed with the results of the vortical structure visualization obtained experimentally by Bricteux et al 2011 for a 3D high-Reynolds number jet**.** In this experimental work a moving window technique is used in the framework of Particle Image Velocimetry (PIV) method to visualise vortex paring in the jet shear layer. Fig.12 shows the results of the visualisation in the jet symmetry plane that appear qualitatively very similar to the results of the 2D simulation (cf. fig.10a,b,d,g).

For a quantitative comparison, the centre mass velocity of the vortex system and the values of first few vortex slip-through periods are compared with the reference analytical solution for point vortices in inviscid flow.

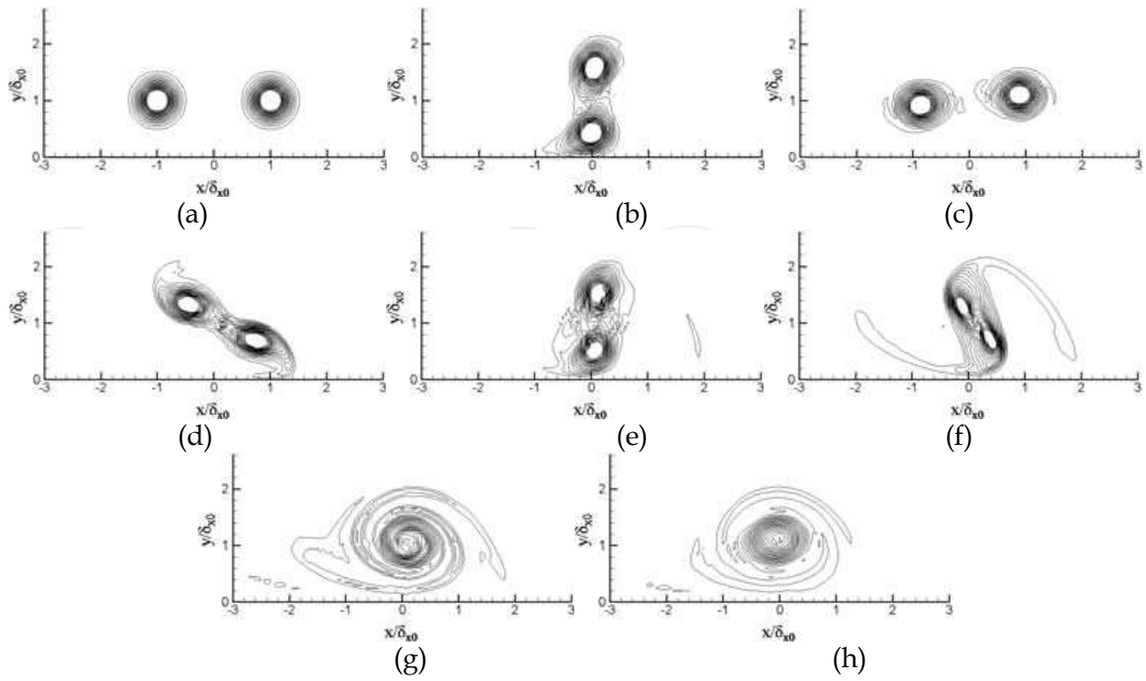

Fig. 10. Vorticity distribution of leapfrogging vortices at several consecutive time moments: $a_\infty t / \delta = 0$ (a), 18 (b), 36 (c), 54 (d), 72 (e), 90 (f), 108 (g), 120 (h).

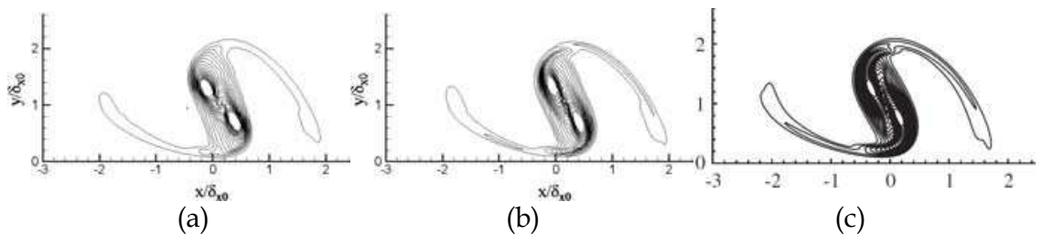

Fig. 11. Vorticity distribution of the leapfrogging vortex pairs at $a_\infty t / \delta = 90$ for (a) CABARET solution with the grid density of 6 cells per vortex core radius, (b) CABARET solution on the grid with 12 cells per vortex core radius, and (c) the reference vortex particle method solution from Eldridge (2007).

Fig. 12. PIV of vorticity distribution of leapfrogging vortex rings in the symmetry plane of a high Reynolds number jet obtained with a moving window technique by Bricteux et al 2011.

Grid spacing, h	$r_0 / 6$	$r_0 / 9$	$r_0 / 12$
$\overline{U}$	0.1271	0.1277	0.1279
$\left(T_p\right)_1$	10.85	10.9	10.9
$\left(T_p\right)_2$	7.9	8.1	8.2

Table 1. Integral characteristics of the vortex system as obtained from the numerical solution

Here $(T_p)_1$ is the time period between the first and the second vortex sleep-through and $(T_p)_2$ is the time period before the second and the third sleep-through. The agreement for the meanflow velocity between the point-vortex theory value (0.1282) and the numerical values on 3 different grids is within 1%. For the sleep-through period, the values obtained on different grids are converged within 0.5%. The numerically predicted time period, however, is 10-15% shorter in comparison with the point-vortex theory (12.21). This discrepancy is within the order of accuracy the point-vortex model, $(r_0/\delta)^2=0.16$ and thus characterises how non-compact the viscous vortex core is in comparison with the distance between the adjacent vortex centres.

In addition to the near-filed, the far-field pressure field has been computed on a circle control surface at distance of 20δ from the vortex centre of vortices. The control surface is located in the same reference system as the centre of mass that moves at a small subsonic speed, $M_\infty = 0.1083$ with respect to the absolute frame. Fig.13 shows the pressure signals obtained at the control points corresponding to 30^0 and 90^0 angle to the flow direction for Re=5000 and 9400 on the grids of different resolution.

The pressure fluctuations are defined with the reference to the pressure field value at infinity, $p_\infty = 1$. The peaks of the pressure signatures correspond to the vortex sleep-through events and the number of the peaks corresponds to the total number of vortex sleep-throughs, respectively. The phase of intense vortex interaction during the vortex pairing is followed by a "calming" period that corresponds to the vortex roll-up after the coalescence. In comparison with the pre-coalescence time history that is dominated by large-time scales the post-coalescence signal is dominated by small-time-scale events.

For the higher Re-number case, the amplitude of the last acoustic "burst" that corresponds to $a_\infty t / \delta \sim 110$ has some 20% higher amplitude in comparison with other peaks. This loud acoustic event corresponds to the last vortex sleep-through, which takes place at $a_\infty t / \delta \sim 90$ and which is well-captured on the grids of different resolution. After the vortex coalescence, the increase of Reynolds number from 5000 to 9400 also leads to a notable prolongation of small-scale acoustic fluctuations in the post-coalescence phase. These effects may be associated with the small spatial structures that are generated shortly before the vortices coalesce (e.g., fig.10f,g) and which are more sensitive to viscous dissipation.

For the pre-coalescence period of vortex evolution, the numerical solutions that correspond to the grids of different resolution are converged within 1-2% for both Reynolds numbers. For the post-coalescence time history, the grid convergence for the high Reynolds-number case, Re=9400, slows down in comparison with the Re=5000 case. For both Re-number cases, however, the CABARET solution on the grid resolution 12 cells per vortex radius appears adequate to capture the fine pressure field fluctuations well.

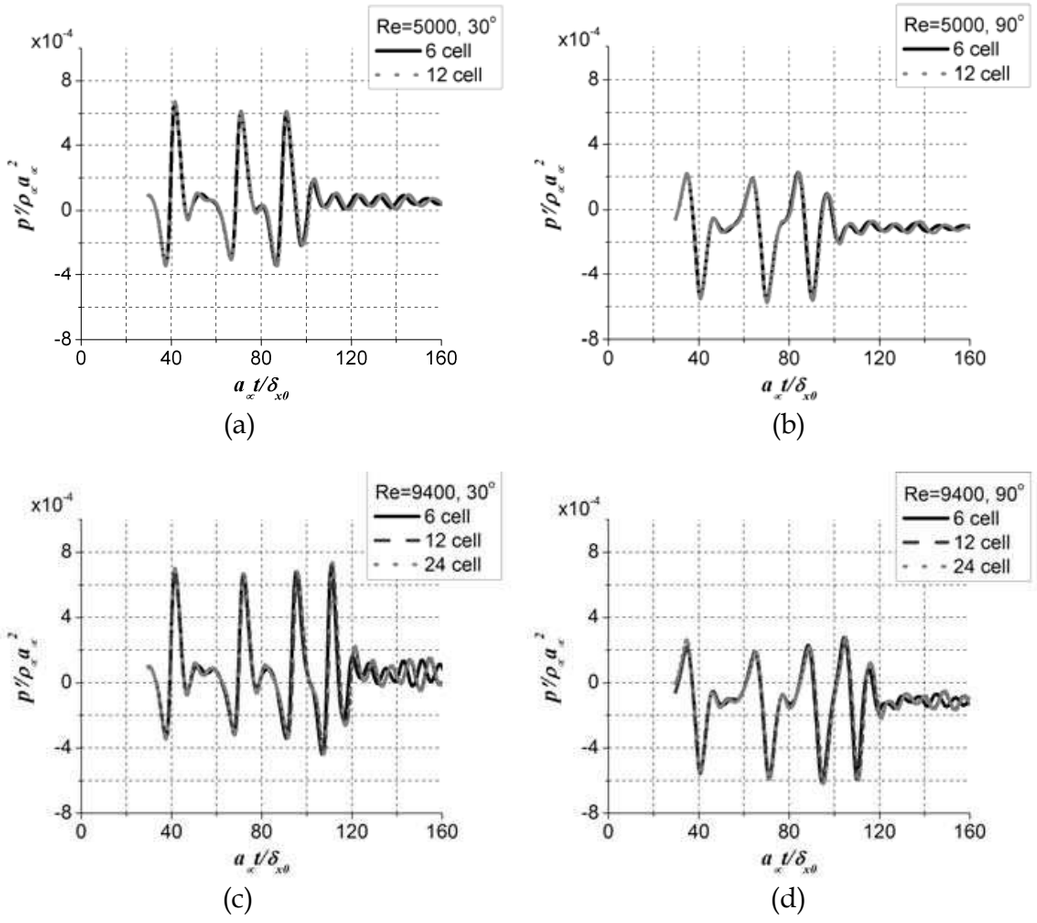

Fig. 13. Acoustic pressure signals at different observer angles to the flow: 30^0 (a),(c) and 90^0 (b),(d) for Re=5000 (a),(b) and Re=9400 (c),(d).

6. Conclusion

The computational of compressible vortical flows is challenging because of the multi-scale phenomena involved. Computational approaches and numerical methods for the solution of compressible vortical flow problems have been discussed. In particular, the key elements of a successful computational method have been outlined that include low numerical dissipation and low dispersion, as well as the good vortex preservation property. For the sake of illustration, several two-dimensional problems are considered that typically present a challenge for conventional Eulerian numerical schemes. The problems include the preservation of steady vortex in a box domain, acoustic wave scattering by a vortex field and the dynamics and acoustics of counter-rotating vortices pairs. For these problems, several computational solutions are presented and discussed, including those obtained with the CABARET scheme developed by the authors. Analytical and reference solutions are provided where applicable. All test problems considered are promoted as the benchmark problems for new Computational Fluid Dynamics codes that are to be used in application for hydrodynamics and acoustics of vortex resolving simulations.

7. References

Bogey, C. and Bailly, C., "A family of low dispersive and low dissipative explicit schemes for flow and noise computations", J. Comput. Physics, 194 (2004), pp. 194-214.

Bogey C. and Bailly C., "Influence of nozzle-exit boundary-layer conditions on the flow and acoustic fields of initially laminar jets", J. Fluid Mech., Vol.25, 2010, pp507-540.

Boris, J.P., Book, D.L., and Hain, K., "Flux-corrected transport: Generalization of the method", J. Comput. Phys, 31,(1975), 335-350.

Bricteux, L., Schram C., Duponcheel M., Winckelmans, G., "Jet flow aeroacoustics at Re=93000: comparison between experimental results and numerical predictions", AIAA-2011-2792, 17th AIAA/CEAS Aeroacoustics Conference (32nd AIAA Aeroacoustics Conference), 6-8 June, Portland, Oregon, 2011

Cockburn B and Shu CW, "Runge–Kutta Discontinuous Galerkin Methods for Convection-Dominated Problems", Journal of Scientific Computing, 16(3): 173-261, Sept 2001.

Colonius T., Lele S.K., and Moin P., "The scattering of sound waves by a vortex: numerical simulations and analytical solutions", J Fluid Mech (1994), 260, pp 271-298.

Colonius T and Lele SK., "Computational aeroacoustics: progress on nonlinear problems of sound generation." Progress in Aerospace sciences, 2004, 40, pp. 345-416.

Dritschel, D.G., Polvani, L.M. and Mohebalhojeh, A.R.: The contour-advective semi-Lagrangian algorithm for the shallow water equations. Mon. Wea. Rev. 127(7), pp. 1551–1565 (1999).

Eldridge, J.D., "The dynamics and acoustics of viscous two-dimensional leapfrogging vortices", J. Sound Vib., 301 (2007) 74–92.

Fritsch G. and Giles M., "Second-order effects of unsteadiness on the performance of turbomachines", ASME Paper 92-GT-389; 1992.

Georges, T.M. "Acoustic ray paths through a model vortex with a viscous core", J.Acoust.Soc. of America, Vol. 51, No. 1 (Part 2) pp. 206-209 (1972).

Goloviznin V.M. and Samarskii, A.A. "Difference approximation of convective transport with spatial splitting of time derivative", Mathematical Modelling, Vol. 10, No 1, pp. 86-100.

Goloviznin V.M. and Samarskii, A.A., "Some properties of the CABARET scheme", Mathematical Modelling, Vol. 10, No 1, 1998, pp. 101–116.

Goloviznin, V.M. "Balanced characteristic method for systems of hyperbolic conservation laws", Doklady. Mathematics, 2005, vol. 72, no1, pp. 619-62313.

Harten, A., Engqist, B., Osher, S., and Chakravarthy, S. "Uniformly High Order Accurate Essentially Non-Oscillatiry Schemes III", J. Comput. Phys, 71, (1987), pp. 231-303.

Hicks, W.M. "On the mutual threading of vortex rings", Proceedings of the Royal Society of London A 10 (1922) 111–131.

Hirsh, C., "Numerical computation of internal and external flows", vol. 2, John Wiley & Sons, 1998.

Howe, M.S., "The generation of sound by aerodynamic sources in an inhomogeneous steady flow", J. Fluid Mech., Vol 67, No. 3, 1975, pp. 597-610.

Inoue, O "Sound generation by the leapfrogging between two coaxial vortex rings", Physics of Fluids 14 (9) (2002) 3361–3364.

Iserles, A. "Generalized Leapfrog Methods", IMA Journal of Numerical Analysis, 6 (1986), 3, 381-392.

Karabasov, S.A., Berloff, P.S. and Goloviznin, V.M. "CABARET in the Ocean Gyres", J. Ocean Model., 30 (2009), pp. 155–168.

Karabasov, S. A. and Goloviznin, V.M.. "A New Efficient High-Resolution Method for Non-Linear problems in Aeroacoustics", AIAA Journal, 2007, vol. 45, no. 12, pp. 2861 – 2871.

Karabasov, S.A. and Goloviznin, V.M. "Compact Accurately Boundary Adjusting high-REsolution Technique for Fluid Dynamics", J. Comput.Phys., 228(2009), pp. 7426–7451.

Kim S., "High-order upwind leapfrog methods for multidimensional acoustic equations", Int J. Numer. Mech. Fluids, 44 (2004), pp. 505-523.

Kinsler, L.E., Frey, A.R., Coppensand, A.B., Sanders, J.V. "Fundamentals of acoustics", Wiley and Sons Inc. (2000).

Kolgan, V.P. "Numerical schemes for discontinuous problems of gas dynamics based on minimization of the solution gradient", Uch. Zap.TsAGI, 1972, v.3, N6, pp.68-77

Kreichnan, R.H., "The scattering of sound in a turbulent medium". J. Acoust. Soc. Am. 25, 1953, pp. 1096-1104.

Lele, S.K., "Compact finite-difference scheme with spectral-like resolution", J.Comput. Physics, 103 (1992), 16-42.

Liu, X.D., Osher, S., and Chan, T., "Weighted essentially non-oscillatory schemes", J.Comp. Phys, 115 (1994), 200-212.

Margolin, L.G. and Shashkov, M. 2004. "Remapping, recovery and repair on a staggered grid", Comput. Methods Appl. Mech. Engng, 193, pp. 4139 – 4155.

Michelassi, V., Wissink, J., Rodi, W. "Direct numerical simulation, large eddy simulation and unsteady Reynolds-averaged Navier-Stokes simulations of periodic unsteady flow in a low-pressure turbine cascade: a comparison. Proc. IMechI, Part A: Journal of Power and Energy, 2003; 217(4), pp. 403-411.

Roe P.L. "Characteristic based schemes for the Euler equations", Annual. Rev. Fluid. Mech. 1986. V.18. pp.337-365.

Roe, P.L. "Linear bicharacteristic schemes without dissipation", SISC, 19, 1998, pp. 1405-1427.

Tam, C.K.W. and Webb. J.C., "Dispersion-relation-preserving finite difference schemes for computational acoustics", J.Comput. Physics, 107 (1993), 262-281

Thompson, K.W. "Time dependent boundary conditions for hyperbolic systems, II." Journal of Computational Physics, 89, pp. 439-461, 1990.

Toro, E.F. "Godunov methods: theory and applications", Kluwer Academic/Plenum Publishers, 2001

Tran, Q.H. and Scheurer, B. "High-Order Monotonicity-Preserving Compact Schemes for Linear Scalar Advection on 2-D Irregular Meshes", J. Comp. Phys. 2002, Vol. 175, Issue 2, pp. 454 - 486.

Tucker, P.G. and Karabasov, S.A. "Unstructured Grid Solution Approach for Eikonal Equation with Acoustics in Mind", International Journal of Aeroacoustics, vol 8 (6), 2009, pp.535-554.

Van Leer B., "Towards the ultimate conservative difference scheme. V. A second-order sequel to Godunov's method", J. Comput. Phys., 32 (1979), pp. 101-136.

Yakovlev P.G., Karabasov, S.A. and Goloviznin, V.M. "On the acoustic super-directivity of jittering vortex systems for the study of jet noise", AIAA-2011-2889, 17th AIAA/CEAS Aeroacoustics Conference (32nd AIAA Aeroacoustics Conference), 6-8 June, Portland, Oregon, 2011.

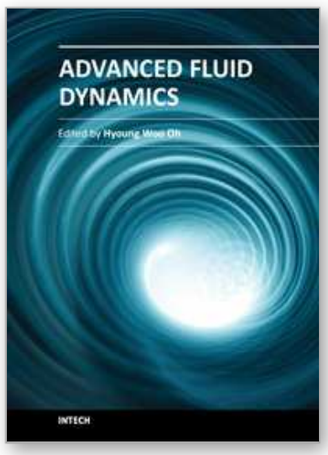

Advanced Fluid Dynamics

Edited by Prof. Hyoung Woo Oh

ISBN 978-953-51-0270-0
Hard cover, 272 pages
Publisher InTech
Published online 09, March, 2012
Published in print edition March, 2012

This book provides a broad range of topics on fluid dynamics for advanced scientists and professional researchers. The text helps readers develop their own skills to analyze fluid dynamics phenomena encountered in professional engineering by reviewing diverse informative chapters herein.

How to reference

In order to correctly reference this scholarly work, feel free to copy and paste the following:

S.A. Karabasov and V.M. Goloviznin (2012). Direct Numerical Simulations of Compressible Vortex Flow Problems, Advanced Fluid Dynamics, Prof. Hyoung Woo Oh (Ed.), ISBN: 978-953-51-0270-0, InTech, Available from: http://www.intechopen.com/books/advanced-fluid-dynamics/direct-numerical-simulations-of-compressible-vortical-flow-problems

INTECH
open science | open minds

InTech Europe
University Campus STeP Ri
Slavka Krautzeka 83/A
51000 Rijeka, Croatia
Phone: +385 (51) 770 447
Fax: +385 (51) 686 166
www.intechopen.com

InTech China
Unit 405, Office Block, Hotel Equatorial Shanghai
No.65, Yan An Road (West), Shanghai, 200040, China
中国上海市延安西路65号上海国际贵都大饭店办公楼405单元
Phone: +86-21-62489820
Fax: +86-21-62489821

IntechOpen